CHEMICAL ENGINEERING RESEARCH AND DESIGN XXX (2014) XXX–XXX

Contents lists available at ScienceDirect

Chemical Engineering Research and Design

journal homepage: www.elsevier.com/locate/cherd

# Effect of nozzle geometry and processing parameters on the formation of nanoparticles using FSP

*H. Torabmostaedi, T. Zhang**

*Faculty of Science, Engineering and Computing, Kingston University, London SW15 3DW, UK*

ABSTRACT

Two numerical models were developed to simulate the sauter mean diameter (SMD) of the droplets during atomization and the growth of particles inside the flame by coagulation and sintering. These models were linked to CFD to simulate flame spray pyrolysis (FSP) process. The effects of reactor geometries and processing parameters on the temperature and velocity profiles, droplet evaporation and particle growth were predicted using the validated computation models. The results show that increasing the oxidant gap size (from 0.1 mm to 0.5 mm) by keeping the dispersion gas pressure drop constant at 1 bar (transonic regime ~310–315 m/s) across the nozzle tip increased the gas to liquid mass ratio (GLMR) by a factor of 6. This reduced the flame height and lowered the residence time of the particles in the high temperature zone of the flame, thus, decreased the sintering rate and the growth of nanoparticles. The results also showed that decreasing the oxygen content of the dispersion gas helped to decrease the peak temperature of the flame and reduced the particle size. The simulation results can be used for the FSP equipment design and process optimization.



*Keywords:* FSP; CFD; Nanoparticles; Aerosol; Particle formation; Agglomeration

## 1. Introduction

One of the most important problems for the extensive usage of nanoparticles in industry is the complexity in producing the particles with high chemical purity and desirable phase and morphology. This challenge is increased in large production when it is necessary to keep the required particle size and low cost. Flame synthesis (Ulrich, 1984; Pratsinis, 1998) was established as a process for making nanoparticles in one step with low cost. Two flame synthesis methods have been developed to produce nanoparticles: (a) vapor-fed flame synthesis (VFS), (Akhtar et al., 1991; Johannessen et al., 2000, 2001; Pratsinis and Spicer, 1998) and (b) flame spray pyrolysis (FSP), (Mädler et al., 2002; Mädler and Pratsinis, 2002; Mueller et al., 2003, 2004a,b; Heine and Pratsinis, 2005; Heine et al., 2006).

In the VFS process, particles are formed from individual atoms or molecules in the gas phase. The formation of particles begins when the precursor gas is going through a chemical reaction. In this method high temperatures are needed to evaporate the precursor and provide the condition for the chemical reaction. In the process, the temperature of the flame varies from 1200 K to 3300 K depends on the type of the oxidizer and the operation conditions. At the early stage, the partic1es are formed by gas-phase nucleation and grow by coagulation (particles collide with each other and stick to form agglomerates) and later they coalesce into larger particles. The shape of the final product is determined by the rates of coalescence and coagulation. If the rate of sintering is faster than that of coagulation, the particles are spherical otherwise irregular agglomerate shape is developed (Kruis et al., 1993).

In FSP (as depicted in Fig. 1), the solution (liquid precursor and fuel) is atomized by using an air-assisted nozzle to form the droplets. The droplets are then evaporated and ignited by using a small pilot flame (i.e. positioned around the nozzle tip) to form solid nanoparticles like VFS after combustion. The FSP became one of the best aerosol synthesis techniques since both organic and inorganic precursors can be used to produce nanoparticles and it has the advantage

* *Corresponding author*. Tel.: +44 02084174703.
E-mail address: t.zhang@kingston.ac.uk (T. Zhang).
Received 15 February 2013; Received in revised form 3 January 2014; Accepted 6 January 2014
0263-8762/$ – see front matter © 2014 The Institution of Chemical Engineers. Published by Elsevier B.V. All rights reserved.
http://dx.doi.org/10.1016/j.cherd.2014.01.011

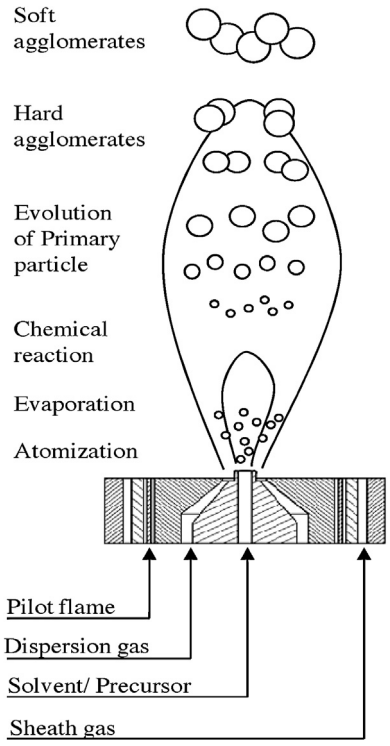


**Fig. 1 – Schematic of FSP apparatus.**

of dissolving precursor directly in the fuel (Mädler et al., 2002).

Large number of studies has been carried out to investigate the effect of FSP parameters on particle purity, phase and morphology. Mädler et al. (2002) investigated the effect of oxidants and mixture compositions on the size of silica primary particles using hexamethyldisiloxane (HMDSO) dissolved in ethanol, iso-octane or methanol. Mädler and Pratsinis (2002) investigated the synthesis of $Bi_2O_3$ by FSP using the same reactor. Mueller et al. (2003, 2004a,b) studied the high production of silica and zirconia. They developed a simple monodisperse model for the coagulation and sintering of zirconia with 10% accuracy in the prediction of the primary and agglomerate particle size by neglecting the effect of particle polydispersity and droplet evaporation. Heine and Pratsinis (2005) incorporated the effect of droplet evaporation by developing a detailed droplet-particle population balance model.

These studies were focused on particle dynamics based on the experimental input data (such as temperature, velocity, and droplet evaporation). Gröhn et al. (2012) investigated the lab scale production of zirconia numerically. Flame temperature validation was performed for pure solvent in the experiment (effect of precursor in the solution was neglected). This would decrease the peak temperature of the flame since the enthalpy of combustion of the solution would decrease by neglecting the precursor (from 25.4 kJ/ml in ETOH/ZP to 21.4 kJ/ml in pure ETOH, Heine et al., 2006). Recently, Torabmostaedi et al. (2013) numerically studied the effect of process parameters on the spray flame structure and the product particle characteristics at medium scale production rates. The prediction for gas dynamics, initial droplet size and final primary particle size in FSP process was validated against the documented experimental measurements (Mueller et al., 2004a,b; Heine et al., 2006). It was shown that the primary particle diameter can be closely controlled at 15.5 nm in medium production rates by creating a constant residence time for zirconia nanoparticles at high temperature zone through a constant gas to liquid flow ratio (GLFR) at low precursor concentration (0.5 M ZP in ethanol).

In FSP process, the physical and chemical properties of nanoparticles depends on a large number of parameters, such as the burner design, atomization, gas-to-liquid-mass-ratio (GLMR), oxygen content of the dispersion gas, fuel and precursor properties, the concentration of the precursor in the solution, etc. To control the phase, particle size and morphology, it is necessary to optimize all of the relevant experimental parameters.

Since measuring the process parameters experimentally is expensive, time consuming and may not be feasible for some parameters (e.g. the growth and agglomeration of particles during the process), the computational fluid dynamics (CFD) may be an alternative tool for optimizing the FSP process. The ability of CFD to predict the performance of a new design before it is manufactured or implemented makes it an integral part of engineering design and analysis. Using CFD and numerical models, the formation and growth of nanoparticles in FSP can be predicted without the need to produce a prototype of equipment and carry out experimental tests. This study is to investigate the effect of nozzle geometry and processing parameters on the growth of zirconia particles using a commercial code, FLUENT, which will predict the multicomponent droplet evaporation, temperature, velocity and gas density in the flame and the results will be compiled into a software developed in our previous study (Torabmostaedi et al., 2013) based on the model developed by Kruis et al. (1993).

Zirconia is studied here due to its wide applications in industry and the available data for the validation. The aim of this study is to provide information and a better understanding on the effect of nozzle geometry and processing parameters on the gas dynamics, droplet vaporization and ultimately the formation and growth of nanoparticles during flame spray pyrolysis.

## 2. Modelling procedures

The effect of oxidizer gap size at a constant pressure drop was investigated based on a production rate of 100 g/h of zirconia. Fig. 2 shows the configuration of the nozzle geometry and computational domain which is consistent with the experimental setup of Heine and Pratsinis (2005) and was fully described by Torabmostaedi et al. in the previous study (Torabmostaedi et al., 2013). The nozzle consists of a capillary tube with a diameter of 0.5 mm for feeding the liquid and an annular gap (x, see Fig. 2) for atomizing the liquid droplets. The annular gap size depends on the desired pressure drop on the working mass flow rate and will vary from 0.1 mm to 0.5 mm. There are three more concentric tubes surrounding the atomizing gas inlet. Methane and oxygen were supplied through the first two annuli to form a diffusion flame for the ignition of the main flame. The last annulus is to provide excess oxygen for the main flame close the nozzle exit. The solution of 0.5 mol zirconium n-propoxide 70 wt% in n-propanol diluted in ethanol was injected into a pre-existing methane–oxygen flame. The solvent(s) then evaporates and combusts to form a high temperature flame. In the flame, chemical reactions and particle growth will take place to produce zirconia nanoparticles.

The modelling of gas dynamics, droplet transport, Turbulence, chemical reaction and radiation has been fully described by Torabmostaedi et al. in previous study

Please cite this article in press as: Torabmostaedi, H., Zhang, T., Effect of nozzle geometry and processing parameters on the formation of nanoparticles using FSP. Chem. Eng. Res. Des. (2014), http://dx.doi.org/10.1016/j.cherd.2014.01.011

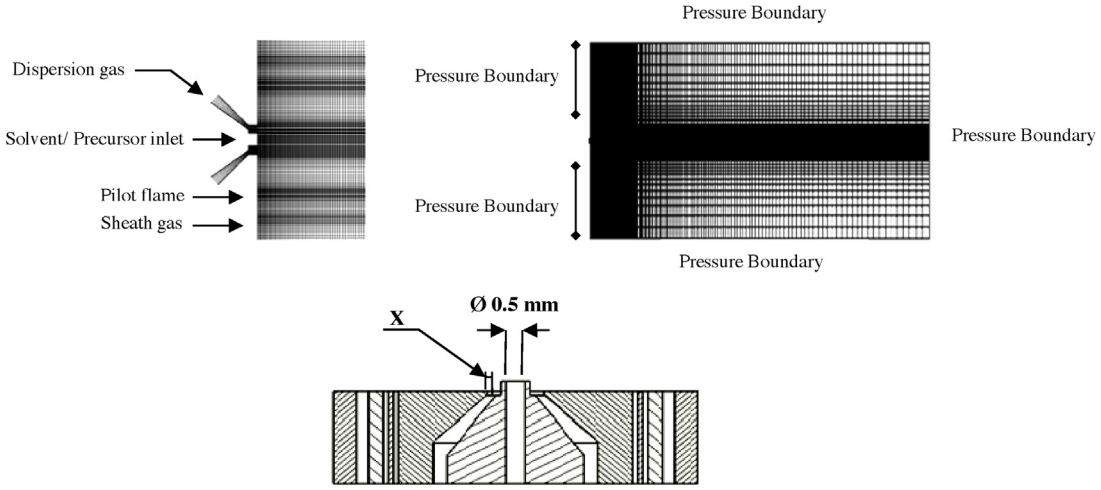


**Fig. 2 – Nozzle geometry and computational domain.**

(Torabmostaedi et al., 2013) and hence only a brief description is given in this paper. In the computation model, the cold gas velocity at the nozzle exit was obtained from the solutions of Navier Stokes equations for the compressible flow. This velocity was then used as an input data to calculate the initial sauter mean diameter of droplets (Elkotb et al., 1982). The effect of radiative heat transfer was included to accounts for both scattering and exchange of radiation between gas and droplets. The history of fuel/precursor droplets was computed with a Lagrangian method, while the Eulerian method was adopted for continuous phase. In order to calculate the evaporation and temperature change of the droplets, the finite inter-phase transport rates and the effects of turbulence interactions between the droplets and continuous phases were considered. The evaporation of multicomponent solution was studied by implementing a user-defined function in FLUENT (Fuchs, 1959; Sazhin, 2006) to calculate the heat and mass transfer of each component between the droplet and the continuous phase.

The particle dynamics were studied using the monodisperse model (Kruis et al., 1993) which solves the coagulation and sintering of particles simultaneously. The simulated centreline density, temperature and velocity profiles were used as an input data in the particle model to determine the particle number concentration, sintering rate and residence time of nanoparticles above the nozzle exit.

## 3. Numerical scheme

The axisymmetric FSP apparatus (Fig. 2) represented by a 2D simulation domain was adopted in this study. The mesh consists of 640 axial nodes and 120 radial nodes. The external region covers 100 cm in length and 15 cm in radius. The grid around the solution and oxidant inlet was successively refined in a grid independent study in order to accurately capture the steep variations in flow properties due to the effects of compressibility of oxidant. A constant pressure condition was used at the outlets of the outside domain (1 atm). The governing equations for the conservation of mass, momentum, energy, turbulence, chemical species, and radiation were solved sequentially by a control volume-based technique. A second-order upwind discretization scheme was used since it ensured the accuracy, stability and convergence. SIMPLEC algorithm (SIMPLE-Consistent) described by Van Doormaal and Raithby (1984) was used for pressure–velocity coupling, which uses a relationship between velocity and pressure corrections to enforce mass conservation and to obtain the pressure field. The appropriate under relaxation factors were imposed to avoid instability in the solution.

## 4. Results and discussion

### 4.1. *Effect of nozzle geometry*

The influence of nozzle geometry on atomization, evaporation, combustion and the growth of zirconia particles were investigated using a fixed solution of 0.5 mol ZP in ethanol at a feeding rate of 27.1 ml/min (100 g/h production of $ZrO_2$). The flow rates of oxidizer (dispersion gas, $O_2$) were controlled by changing the oxidizer gap sizes at fixed pressure drop across the nozzle tip. The mass flow rates of dispersion gas for different gap sizes (X1–X5) at a constant pressure drop of 1 bar across the nozzle tip are given in Table 1. The mass flow rate of dispersion gas increased from 11 l/min to 64 l/min as the gap size increased from 0.1 mm to 0.5 mm, respectively. This corresponds to a direct effect on the gas to liquid mass ratio (GLMR) by a factor of 6.

#### 4.1.1. *Temperature distribution*

Fig. 3 shows the calculated centreline flame temperatures at a constant pressure drop of 1 bar across the nozzle tip for various gap sizes for dispersion gas. The temperature in all cases increases rapidly (up to 3250 K) at the initial stage and decreases slowly when the distance from the nozzle exit is increased. The results show that increasing the flow rate of dispersion gas from 11 l/min to 64 l/min increases the quenching rate and consequently decreases the flame height. The flame height (calculated as axial position where the temperature reduced to 1500 K, (Mueller et al., 2004a)) decreased from 25 cm to 11 cm for X1 and X5, respectively.

**Table 1 – Operating conditions at different oxidizer gap size.**

| Flame | X1 | X2 | X3 | X4 | X5 |
|---|---|---|---|---|---|
| Gap size (mm) | 0.1 | 0.2 | 0.3 | 0.4 | 0.5 |
| Pressure drop (bar) | | | 1 | | |
| Dispersion gas flow rate (l/min) | 11 | 23 | 36 | 50 | 64 |
| GLMR | 0.64 | 1.4 | 2.1 | 3 | 3.8 |

Please cite this article in press as: Torabmostaedi, H., Zhang, T., Effect of nozzle geometry and processing parameters on the formation of nanoparticles using FSP. Chem. Eng. Res. Des. (2014), http://dx.doi.org/10.1016/j.cherd.2014.01.011

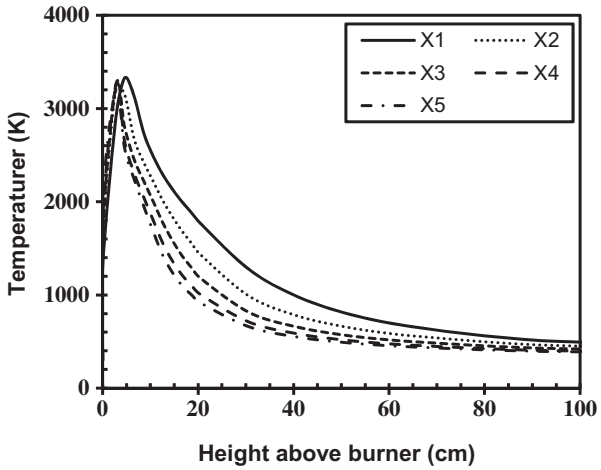


**Fig. 3 – The temperature at the centreline of five flame configurations.**

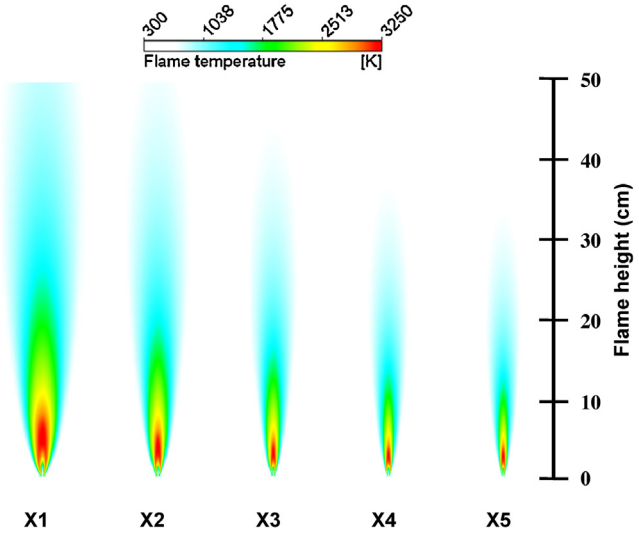


**Fig. 4 – Temperature contours at different flame configurations.**

The temperature profiles of the flames are strongly influenced by the combustion, which depends on the availability of fuel and oxygen. Fig. 4 shows the high temperature zone of flame moves closer to the nozzle exit when the GLMR increased from 0.64 to 3.8 for X1 and X5, respectively. This is a direct result of the increase of supplied oxidant to the reaction zone which intensifies the mixing of fuel and oxygen and the reduction of droplet size due to the increase of GLMR. This will be discussed further in next section.

Fig. 5 shows the mass fractions of the fuel mixture and oxygen as a function of the distance to the nozzle exit along the centreline of the nozzle axis. After ignition, the flame mixes with the surrounding air and more oxygen gradually diffuses into the flame. The diffused oxygen reacts with the non reacted fuel mixture, which gradually decreases the mass fraction of fuel mixture. When the combustion reaction is completed, the temperature starts to decrease continuously. This behavior can be seen in Fig. 5, which shows the mass fractions of oxygen and the fuel mixture above the nozzle exit. The simulation results show that, with the increase of gap size from X1 to X5, the mass fraction of oxygen increases rapidly while the mass fraction of the fuel mixture (ETOH/ZP) decreases. The computed oxygen mass fraction along the flame centreline increased from nearly zero at the tip of the liquid nozzle, and started to rise at different height above nozzle in cases X1–X5, where most of the fuels are decomposed and oxygen slowly diffuse into the flame. These results are in agreement with the turbulent (Pitsch et al., 1998) and laminar (Joo and Gülder, 2010) diffusion flame studies, where in the lean part of the flame (i.e. close to the nozzle exit along the centreline) the oxygen mass fraction is too low.

In X1, the oxygen content is less than 1% at 60 mm above the nozzle exit. This region decreased to 25 mm for X5 as a result of higher oxygen/dispersion gas feeding rate. The combustion rate in this region is determined by the availability of oxygen. The second region starts after the completion of oxidation of the fuel mixture. The gas temperature begins to decrease since there is no fuel left to react with the entrapped air. At a distance of 200 mm above the nozzle exit, the mass fraction of oxygen is still below its value in air (0.232) for X1 and X2. This indicates the existence of unburned fuel which is still reacting with the entrapped air. This distance (oxygen content 0.232) is decreased to 104, 70 and 64 mm for X3, X4 and X5, respectively.

Fig. 5b shows the mass fractions of ETOH and ZP above the nozzle exit. The peak mass fraction for ETOH and ZP appears at different positions. This is because the most volatile species (ETOH) vaporizes at the droplet surface and less volatile species (ZP) vaporizes afterwards. This will be discussed further in next section. For this reason, the oxidation of ethanol begins at close to the nozzle exit while the ZP oxidation starts at a longer distance above the nozzle exit. Since the oxidation

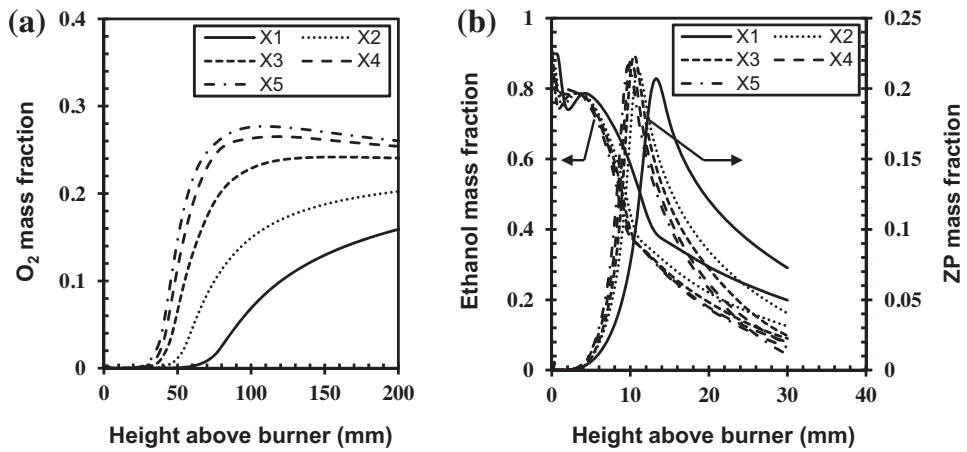


**Fig. 5 – Effect of different nozzle configurations on the centreline mass fractions of (a) oxygen and (b) mixture fuel.**

Please cite this article in press as: Torabmostaedi, H., Zhang, T., Effect of nozzle geometry and processing parameters on the formation of nanoparticles using FSP. Chem. Eng. Res. Des. (2014), http://dx.doi.org/10.1016/j.cherd.2014.01.011

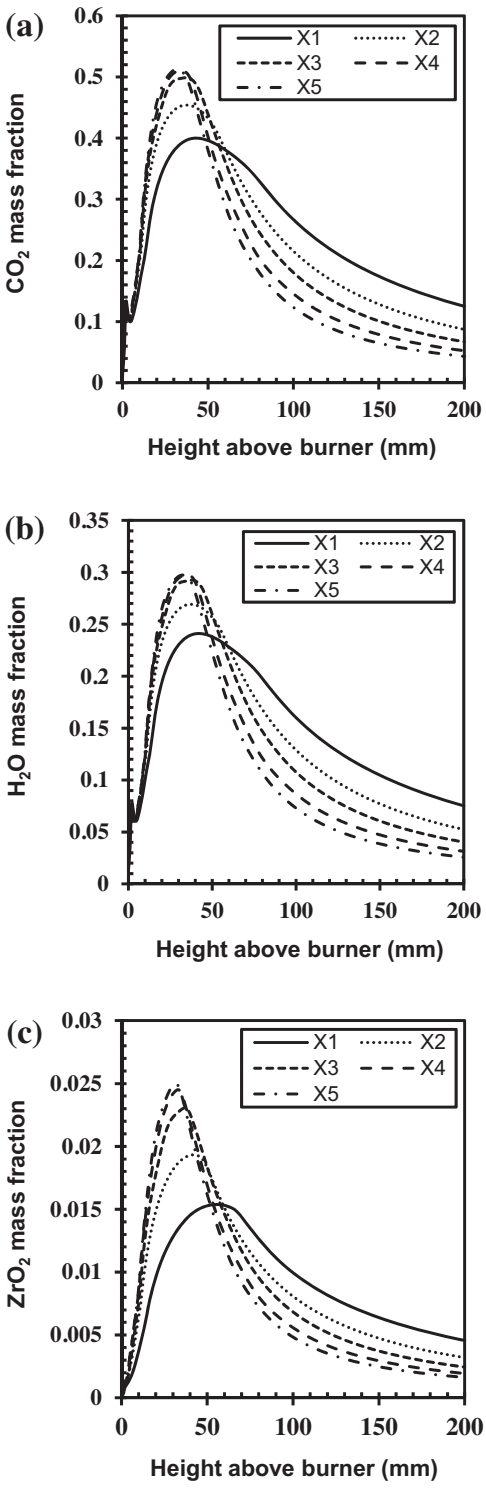


**Fig. 6 – Effect of GLMR on (a) $CO_2$ mass fraction; (b) $H_2O$ mass fraction and (c) $ZrO_2$ mass fraction.**

of the precursor is the initial stage of the zirconia formation, the reaction height affects the formation and the growth of nanoparticles.

To understand the effects of GLMR on the flame profile, the axial distribution of combustion products ($CO_2$, $H_2O$ and $ZrO_2$) along the centreline of the flame for different configurations were calculated and presented in Fig. 6. The peaks of the mass fractions for all the combustion products increased and shifted slightly towards the nozzle exit when the gap size was increased. The production rate of the combustion products strongly depends on the availability of the oxygen. The higher oxygen content at near to the nozzle exit accelerates the consumption of fuel mixture and the production of nanoparticles. The locations of the peak mass fraction of $CO_2$, $H_2O$ and $ZrO_2$ for the X1 flame are at 43, 42 and 55 mm above the burner, respectively. This distance reduced to 32 mm for all the products in X5. As the formation of products getting closer to the nozzle exit, the peak temperature and the flame height are reduced (see Figs. 3 and 4).

#### 4.1.2. *Droplet evaporation*

Fig. 7a shows the calculated sauter mean diameter of ETOH/ZP droplets as a function of distance from nozzle exit for the oxidant gap sizes of 0.1, 0.2, 0.3, 0.4 and 0.5 mm (cases X1–X5) at the zirconia production of 100 g/h. The droplet evaporation length is the shortest for the X5, due to its smallest droplet size. This implies that large gap size will lead to a higher gas to liquid mass ratio, smaller droplet size, higher droplet surface area, and faster vaporization, fuel–air mixing and oxidation of components. The evaporation height for the mixture of droplets decreased from 14 mm to 10.5 mm for X1 and X5, respectively. In the flame, the most volatile species (ETOH) vaporize at the droplet surface and the less volatile species (ZP) vaporizes later (Sirignano, 2009). Fig. 7b shows the reduction of droplet sizes as a function of temperature for X1–X5. In all cases, ethanol evaporates first due to its lower boiling temperature (350 K). As the temperature increases, 1-propanol and zirconium n-propoxide evaporate at 370 and 480 K, respectively. The earlier evaporation of the precursor droplets in X5 resulted in earlier oxidation of the fuel mixture (see Fig. 5b), thus, lowered the flame height (see Fig. 4).

#### 4.1.3. *Flame gas velocity*

Flame gas velocity determines the residence time of the primary particles in the flame. The higher is the flame velocity, the lower is the residence time for the particles in the high temperature zone of the flame, which will lead to a lower growth of particle size. However, if the residence time of droplets in the flame is too low it will result in an incomplete conversion of the precursor to the desired particle phase. In this study the pressure drop was kept constant at 1 bar which results in a transonic regime (~310–315 m/s) at the dispersion gas exit.

Fig. 8a shows the centreline velocities of five different flame configurations shown in Table 1. The gas velocity profiles along the centreline exhibit two regions for all the configurations. The velocity profiles exhibit a sudden increase at the initial stage and followed by a rapid decay in the second region. The expansion of gas velocity in the first region can be explained by the evaporation and combustion of ETOH/ZP droplets. In the second region, the gas velocity decreases with height, since more ambient air is entrained (see Fig. 5a). The entrapped air has lower momentum and cools the flame. Since the pressure drop was kept constant, the velocity of the dispersion gas at the nozzle exit was constant for all flame configurations.

At above the nozzle exit, the flame velocity is proportion to the mass flow rate of the dispersion gas. Higher oxidant flow rate intensifies the fuel–oxygen mixing and increases the burning rate of ETOH/ZP droplets which brings the reaction zone closer to the nozzle exit (Fig. 8b) and results in a higher peak velocity. The peak centreline velocity increased from 53 m/s to 149 m/s when the gap size was increased from 0.1 mm (X1) to 0.5 mm (X5). Fig. 9 shows the radial distribution of the gas velocity at five different axial locations of $L = 10$, 50, 100, 150 and 200 mm for two cases (X1 and X5). At close to the

Please cite this article in press as: Torabmostaedi, H., Zhang, T., Effect of nozzle geometry and processing parameters on the formation of nanoparticles using FSP. Chem. Eng. Res. Des. (2014), http://dx.doi.org/10.1016/j.cherd.2014.01.011

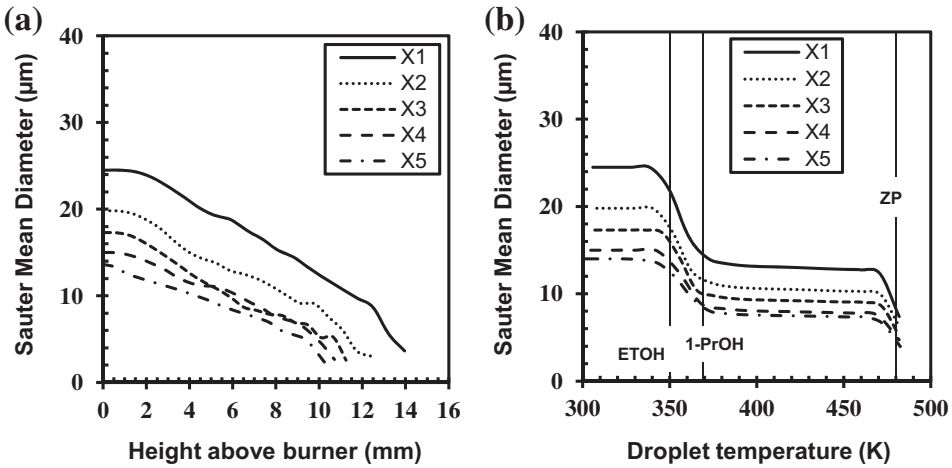


**Fig. 7 – Droplet size evolution (a) sauter mean diameter calculated above the burner and (b) droplet mass reduction as a function of temperature.**

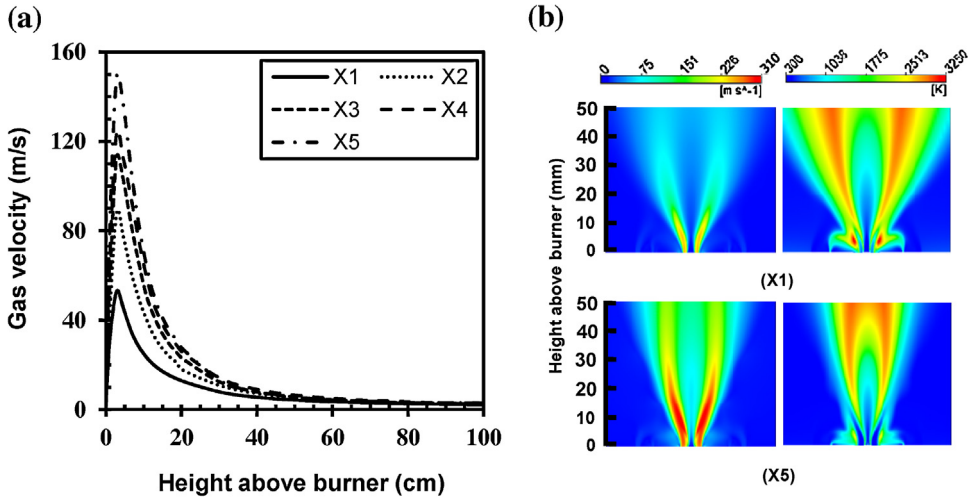


**Fig. 8 – The effect of oxidant gap size on (a) centreline velocity and (b) velocity (LHS) and temperature (RHS) contour plots at 50 mm height above the burner for X1 and X5.**

nozzle exit ($L$ = 10 mm), the position of the maximum velocity is about 3 mm away from the central axis which was caused by the expansion of gases after combustion (see Fig. 8b). At this height, the distributions of gas velocity are in steep saddle shapes in the vicinity of the nozzle exit and it suddenly changes to a sloped saddle shape and then becomes flat as the flame propagates downstream. The peak value of the velocity at $L$ = 10 mm is at a position inside the flame where the fuel mass fraction is high (combustion just started) (see Fig. 5b). This value increased from 82 m/s to 216 m/s for X1 and X5, respectively. At higher height above the nozzle exit ($L$ = 50, 100, 150 and 200 mm), the maximum velocity is at the centre of the flame and it gradually decreases with increasing the radial distance and goes down to 0 m/s at about 40 mm away from the centre.

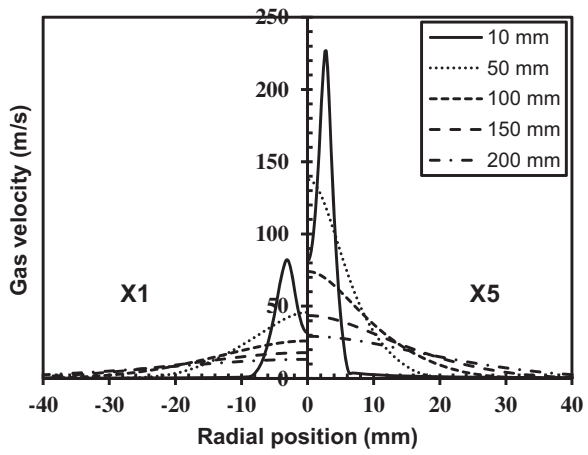


**Fig. 9 – Radial distribution of gas velocity at different height above the burner for X1 (LHS) and X5 (RHS).**

#### 4.1.4. *Particle growth*

The evolution of the zirconia primary particles for the flames (X1–X5) were calculated and the results are given in Fig. 10a. The sintering rate is a function of flame temperature (Fig. 3), velocity (Fig. 8a) and height (Fig. 4). As the flame configuration is changed from X1 to X5, the growth rate of particles decreased by a factor of 2.5. This can be explained by the lower flame height (Fig. 4) and higher gas velocity (Fig. 8a) which decrease the residence time of particles in the flame and lower the particle growth (Fig. 10a).

In X1, it can be seen that after an initial rapid rise, caused by fast coalescence, the primary particles stop growing and reach a constant value of 31 nm at 38 cm above the nozzle exit. The primary particle size decreased as the gap size is increased. Increasing the gap size to 0.5 mm (X5) decreased the particle

Please cite this article in press as: Torabmostaedi, H., Zhang, T., Effect of nozzle geometry and processing parameters on the formation of nanoparticles using FSP. Chem. Eng. Res. Des. (2014), http://dx.doi.org/10.1016/j.cherd.2014.01.011

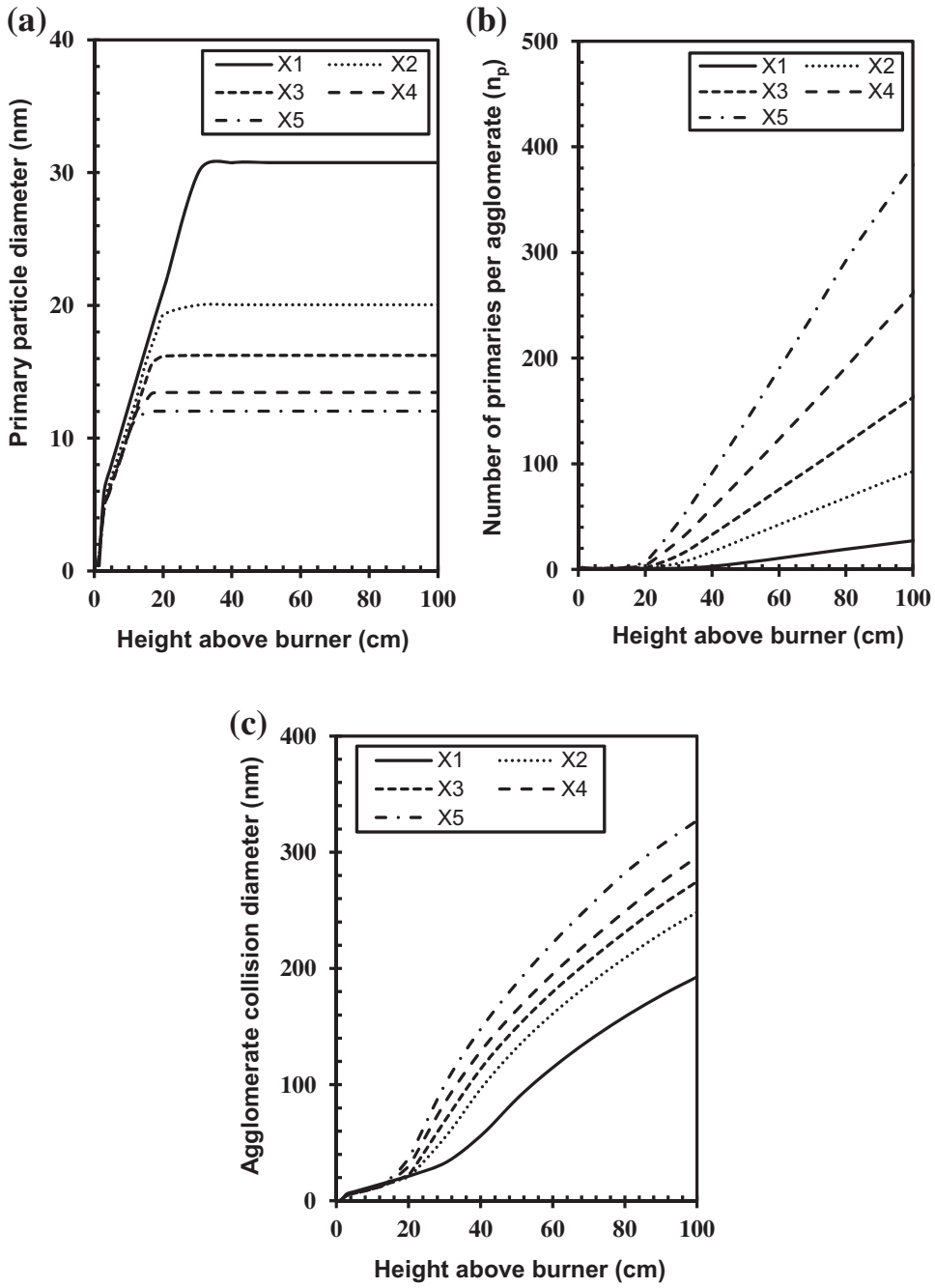


**Fig. 10 – Evolution of zirconia (a) primary particle diameter, (b) number of primary particles per agglomerate and (c) agglomerate collision diameter predicted by the proposed model at different flame configurations.**

size to 12 nm at 17 cm above the nozzle exit. In all cases, the growth of particles was increased by increasing the temperature and was reduced by decreasing the temperature. This can be further examined by comparing the primary particle profiles of the flames (X1–X5) given in Fig. 10a with their corresponding flame temperature profiles given in Fig. 3. It can be seen that in all cases, the growth of particles stopped when the temperature dropped to below 1400 K. This is the region where the coagulation rate is much higher than the sintering rate.

Fig. 10b shows the evolution of the number of primary particles per aggregate, $n_p$, which was predicted using the flame temperature profile (Fig. 3), velocity (Fig. 8a) and taking the droplet evaporation (Fig. 7a) into account. The $n_p$ value varies in all cases at two regions of the flames, 1) $n_p = 1$, in the reaction zone (temperatures above 1800 K) where the sintering rate is higher than coagulation rate; therefore, all the particles are spherical, 2) $n_p > 1$, after the high temperature zone (below 1800 K) of the flame when the temperature decreasing (less sintering). The $n_p$ increased from 27.4 to 385 while the primary particle diameter decreased from 31 nm to 12 nm for X1 and X5, respectively. This therefore has the direct effect by a factor 1.7 on collision agglomerate diameter (Fig. 10c). Agglomerate formation enhanced by increasing the cooling rate of the flame from X1 to X5 due to the smaller primary particles and the higher number of primaries per agglomerate.

### 4.2. *Effect of oxidant composition*

The effect of oxidant/dispersion gas composition on the flame structure and particle size during FSP was investigated using 0.5 M ZP in ethanol by keeping the volume flow rates of the precursor and dispersion gas constant. Series of cases were defined in order to vary the oxygen content of the dispersion

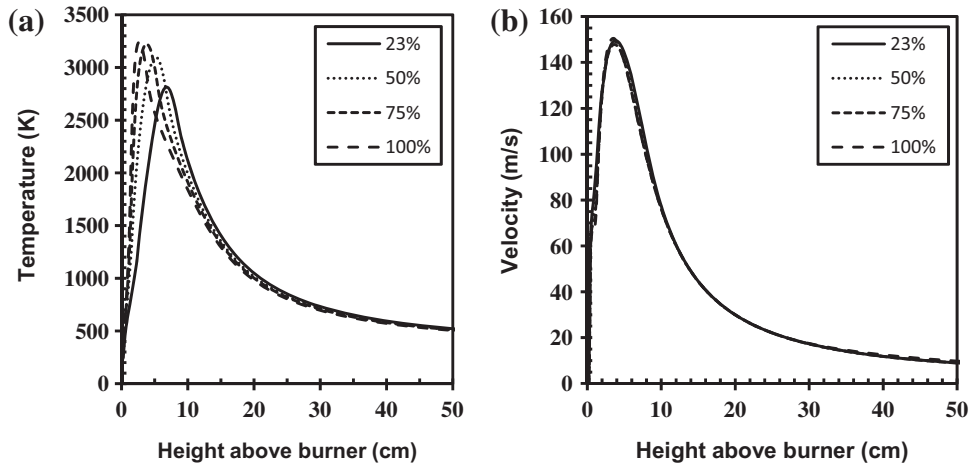


**Fig. 11 – Profiles of (a) temperature and (b) velocity; predicted by proposed model for X5 at different oxidant/dispersion gas composition.**

**Table 2 – Operating conditions at different oxidant/dispersion composition.**

| Flame | X5 | | | |
|---|---|---|---|---|
| Oxygen content (%) | 23 | 50 | 75 | 100 |
| Pressure drop (bar) | | 1 | | |
| Dispersion gas flow rate (l/min) | | 64 | | |
| ETOH/ZP flow rate (ml/min) | | 27.1 | | |

gas from 23% to 100% (see Table 2). Fig. 11 shows the calculated centreline flame temperatures and velocities at different oxidant composition for the flame X5. In comparison, increasing the oxygen content from 23% to 100% increased the quenching rate and consequently decreased the flame height. This is a direct result of the higher oxygen availability close to the nozzle exit which intensified the mixing of precursor solution and oxidant.

The maximum flame temperature is also affected by the composition of the dispersion gas. Using air (23% oxygen content) as dispersion gas, the temperature steadily increases up to 2800 K at 7 cm above the nozzle exit. In the case of pure oxygen (100% oxygen content) the temperature rises up to 3250 K at 3 cm above the nozzle exit. This difference in the maximum temperatures for the different dispersion gas would greatly affect the size of product particles. Fig. 11b shows the gas velocities along the centreline of the spray flames calculated for different oxidant/dispersion gas compositions. Since the volume flow rate of the dispersion gas and the precursor solution was kept constant, the peak flame velocity and the velocity profiles of spray flames at above the nozzle exit are the same. Fig. 12 shows the particle size decreased from 12 nm to 9 nm when the oxygen content of the dispersion gas was decreased from 100% to 23%. Decreasing the oxygen content of the dispersion gas helped to reduce the flame temperatures at above the nozzle exit while keeping the residence time of particles constant. This is a great feature for design optimization in FSP.

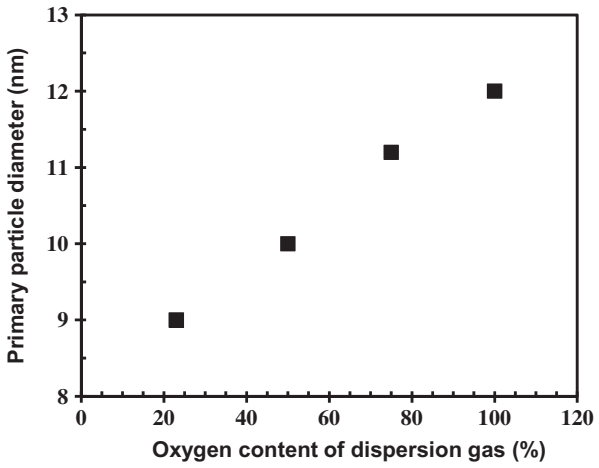


**Fig. 12 – Effect of oxidant/dispersion gas composition on the predicted primary particle diameter for X5.**

## 5. Conclusion

The effects of burner geometries and processing parameters of FSP reactors on the temperature, velocity profiles were investigated using a commercial CFD code, FLUENT. The simulation results were compiled into a numerical model to solve the coagulation and sintering equations to predict the formation of nanoparticles. The initial droplet diameters were predicted using a correlation model for external gas-assisted sprays. The results show that increasing the gap size of the dispersion gas resulted in higher oxidant flow rate which intensified the fuel–oxygen mixing and moved the reaction zone closer to the nozzle exit. This resulted in lower flame height and reduced the residence time of particles in the high temperature zone of the flame. Increasing the dispersion gas flow rate will result in a shorter flame, higher flame velocity and lower residence time for the primary particles in the high temperature zone of the flame which will be able to control the growth rate of primary particles. Finally, it was shown how the primary particle diameter can be decreased to less than 10 nm by decreasing the oxygen content of the dispersion gas while keeping the volume flow rate of the dispersion gas and the precursor solution constant. The results show that the computation model can be used to predict the effects of burner geometries and processing parameters on the formation of particles and thus used for equipment design and process optimization.

Please cite this article in press as: Torabmostaedi, H., Zhang, T., Effect of nozzle geometry and processing parameters on the formation of nanoparticles using FSP. Chem. Eng. Res. Des. (2014), http://dx.doi.org/10.1016/j.cherd.2014.01.011

## Acknowledgements

The research leading to these results has received funding from the European Community's Seventh Framework Programme (FP7/2007-2013) under grant agreement no. 228885.

## References

Akhtar, M.K., Xiong, Y., Pratsinis, S.E., 1991. Vapor synthesis of titania powder by titanium tetrachloride oxidation. AIChE Journal 37 (10), 1561–1570.

ANSYS Fluent, 2010. Release 13.0. ANSYS, Inc.

Elkotb, M.M., Madhy, M.A., Montaser, M.E., 1982. Investigation of external-mixing airblast atomizers. In: Proceedings of the 2nd International Conference on Liquid Atomization and Sprays, Madison, pp. 105–115.

Fuchs, N.A., 1959. Evaporation and Droplet Growth in Gaseous Media. Pergamon Press, London.

Gröhn, A.J., Pratsinis, S.E., Wegner, K., 2012. Fluid-particle dynamics during combustion spray aerosol synthesis of $ZrO_2$. Chemical Engineering Journal 191, 491–502.

Heine, M.C., Madler, L., Jossen, R., Pratsinis, S.E., 2006. Direct measurement of entrainment during nanoparticle synthesis in spray flames. Combustion and Flame 144 (4), 809–820.

Heine, M.C., Pratsinis, S.E., 2005. Droplet and particle dynamics during flame spray synthesis of nanoparticles. Industrial and Engineering Chemistry Research 44 (16), 6222–6232.

Johannessen, T., Pratsinis, S.E., Livbjerg, H., 2000. Computational fluid-particle dynamics for the flame synthesis of alumina particles. Chemical Engineering Science 55 (1), 177–191.

Johannessen, T., Pratsinis, S.E., Livbjerg, H., 2001. Computational analysis of coagulation and coalescence in the flame synthesis of titania particles. Powder Technology 118 (3), 242–250.

Joo, H.I., Gülder, Ö.L., 2010. Soot formation and temperature structure in small methane–oxygen diffusion flames at subcritical and supercritical pressures. Combustion and Flame 157, 1194–1201.

Kruis, F.E., Kusters, K.A., Pratsinis, S.E., Scarlett, B., 1993. A simple model for the evolution of the characteristics of aggregate particles undergoing coagulation and sintering. Aerosol Science and Technology 19 (4), 514–526.

Mädler, L., Kammler, H.K., Mueller, R., Pratsinis, S.E., 2002. Controlled synthesis of nanostructured particles by flame spray pyrolysis. Journal of Aerosol Science 33 (2), 369–389.

Mädler, L., Pratsinis, S.E., 2002. Bismuth oxide nanoparticles by flame spray pyrolysis. Journal of the American Ceramic Society 85 (7), 1713–1718.

Mueller, R., Jossen, R., Kammler, H.K., Pratsinis, S.E., Akhtar, M.K., 2004a. Growth of zirconia particles made by flame spray pyrolysis. AIChE Journal 50 (12), 3085–3094.

Mueller, R., Jossen, R., Pratsinis, S.E., Watson, M., Akhtar, M.K., 2004b. Zirconia nanoparticles made in spray flames at high production rates. Journal of the American Ceramic Society 87, 197–202.

Mueller, R., Mädler, L., Pratsinis, S.E., 2003. Nanoparticle synthesis at high production rates by flame spray pyrolysis. Chemical Engineering Science 58 (10), 1969–1976.

Pitsch, H., Chen, M., Peters, N., 1998. Unsteady flamelet modeling of turbulent hydrogen–air diffusion flames. Symposium (International) on Combustion 27, 1057–1064.

Pratsinis, S.E., 1998. Flame aerosol synthesis of ceramic powders. Progress in Energy and Combustion Science 24 (3), 197–219.

Pratsinis, S.E., Spicer, P.T., 1998. Competition between gas phase and surface oxidation of $TiCl_4$ during synthesis of $TiO_2$ particles. Chemical Engineering Science 53 (10), 1861–1868.

Sazhin, S.S., 2006. Advanced models of fuel droplet heating and evaporation. Progress in Energy and Combustion Science 32, 162–214.

Sirignano, W.A., 2009. Fluid dynamics and transport of droplets and sprays. Cambridge University Press, Cambridge.

Torabmostaedi, H., Zhang, T., Foot, P., Dembele, S., Fernandez, C., 2013. Process control for the synthesis of $ZrO_2$ nanoparticles using FSP at high production rate. Powder Technology 246, 419–433.

Ulrich, G.D., 1984. Flame synthesis of fine particles. Chemical and Engineering News 62 (32), 22–29.

Van Doormaal, J.P., Raithby, G.D., 1984. Enhancements of the simple method for predicting incompressible fluid flows. Numerical Heat Transfer 7 (2), 147–163.

Please cite this article in press as: Torabmostaedi, H., Zhang, T., Effect of nozzle geometry and processing parameters on the formation of nanoparticles using FSP. Chem. Eng. Res. Des. (2014), http://dx.doi.org/10.1016/j.cherd.2014.01.011